

The July 2019 European Heat Wave in a Warmer Climate: Storyline Scenarios with a Coupled Model Using Spectral Nudging

ANTONIO SÁNCHEZ-BENÍTEZ,^a HELGE GOESSLING,^a FELIX PITHAN,^a TIDO SEMMLER,^a AND THOMAS JUNG,^{a,b}

^a Alfred Wegener Institute Helmholtz-Center for Polar and Marine Research, Bremerhaven, Germany

^b Institute of Environmental Physics, University of Bremen, Bremen, Germany

(Manuscript received 24 July 2021, in final form 28 January 2022)

ABSTRACT: Extreme weather events are triggered by atmospheric circulation patterns and shaped by slower components, including soil moisture and sea surface temperature, and by the background climate. This separation of factors is exploited by the storyline approach in which an atmospheric model is nudged toward the observed dynamics using different climate boundary conditions to explore their influence. The storyline approach disregards uncertain climatic changes in the frequency and intensity of dynamical conditions, focusing instead on the thermodynamic influence of climate on extreme events. Here we demonstrate an advanced storyline approach that employs a coupled climate model (AWI-CM-1-1-MR) in which the large-scale free-troposphere dynamics are nudged toward ERA5 data. Five-member ensembles are run for present-day (2017–19), preindustrial, +2-K, and +4-K climates branching off from CMIP6 historical and scenario simulations of the same model. In contrast to previous studies, which employed atmosphere-only models, feedbacks between extreme events and the ocean and sea ice state, and the dependence of such feedbacks on the climate, are consistently simulated. Our setup is capable of reproducing observed anomalies of relevant unconstrained parameters, including near-surface temperature, cloud cover, soil moisture, sea surface temperature, and sea ice concentration. Focusing on the July 2019 European heat wave, we find that the strongest warming amplification expands from southern to central Europe over the course of the twenty-first century. The warming reaches up to 10 K in the 4-K-warmer climate, suggesting that an analogous event would entail peak temperatures around 50°C in central Europe.


SIGNIFICANCE STATEMENT: This work explores a new storyline method to determine the impact of climate change on specific recent extreme events. The observed evolution of the large-scale atmospheric circulation is imposed in a coupled climate model. Variations in climate parameters, including ocean temperatures and sea ice, are well reproduced. By varying the background climate, including CO₂ concentrations, it is demonstrated how the July 2019 European heat wave could have evolved in preindustrial times and in warmer climates. For example, up to 10°C warmer peak temperatures could occur in central Europe in a 4°C warmer climate. The method should be explored for other types of extreme events and has the potential to make climate change more tangible and to inform adaptation measures.


KEYWORDS: Atmospheric circulation; Extreme events; Sea surface temperature; Summer/warm season; Climate change; Soil moisture; Thermodynamics; Climate models; Coupled models; Ensembles

1. Introduction

Europe has recently experienced a number of exceptional heat waves (e.g., Russo et al. 2015; Vautard et al. 2020). These extreme events matter for society as they are associated, among others, with extensive crop failures (Lesk et al. 2016; Beillouin et al. 2020), devastating wildfires (Sutanto et al. 2020), poor air quality (e.g., Kononov et al. 2011; Garrido-Perez et al. 2019), and increased mortality, especially among

older people (Barriopedro et al. 2011; CRED 2020). The most extensively documented heat waves—in terms of studying both the underlying dynamics and the associated impacts—are the August 2003 heat wave over western and central Europe (e.g., Trigo et al. 2005; Russo et al. 2015; Bador et al. 2017) and the July–August 2010 event in western Russia (e.g., Barriopedro et al. 2011; Dole et al. 2011). These heat waves redrew the temperature record map of Europe. More recently, the 2019 summer was exceptional in western and central Europe (Mitchell et al. 2019; Madruga De Brito et al. 2020; Sousa et al. 2020; Vautard et al. 2020) with two large-scale heat waves occurring in late June and July 2019. These two extreme events were found to be the world's deadliest disaster of 2019 (CRED 2020). The former set a new record for the European-average June temperature. The most

 Supplemental information related to this paper is available at the Journals Online website: <https://doi.org/10.1175/JCLI-D-21-0573.s1>.

 Denotes content that is immediately available upon publication as open access.

Corresponding author: Antonio Sánchez-Benítez, antonio.sanchez.benitez@awi.de



This article is licensed under a [Creative Commons Attribution 4.0 license](http://creativecommons.org/licenses/by/4.0/) (<http://creativecommons.org/licenses/by/4.0/>).

DOI: 10.1175/JCLI-D-21-0573.1

© 2022 American Meteorological Society. For information regarding reuse of this content and general copyright information, consult the [AMS Copyright Policy](https://www.ametsoc.org/PUBSReuseLicenses/) (www.ametsoc.org/PUBSReuseLicenses/).

extreme daily maximum 2-m air temperature (t2m) was recorded on 28 June near the city of Nîmes (Verargues; 46°C) in France, where a new all-time national record for France was established. The latter resulted in record-breaking temperatures in central and northern Europe. For example, the historical record of Paris was broken by more than 2°C (42.6°C), Belgium and the Netherlands for the first time surpassed the 40°C mark, and new national records were set in Germany, Luxembourg, and the United Kingdom.

There is consensus that large-scale dynamics, characterized by subtropical ridges and blocking anticyclones associated with meandering of the jet stream, are the main driving factor for European heat waves (e.g., Trigo et al. 2005; Jézéquel et al. 2018; Sánchez-Benítez et al. 2018; Sousa et al. 2020; Suarez-Gutierrez et al. 2020) as warm-air advection from lower latitudes, solar radiative heating, and subsidence are enhanced. The 2003 and 2019 heat waves were associated with a subtropical ridge in western Europe together with a low pressure system in the eastern Atlantic Ocean. This configuration advected hot and dry Saharan and Iberian air masses toward higher latitudes. Soil-atmosphere feedbacks impacted the strength of the heat waves (e.g., van der Wiel et al. 2020) as they generate changes in the surface heat fluxes (Wehrli et al. 2018; Miralles et al. 2019; Sousa et al. 2020). In fact, the heat waves in August 2003 and July 2019 were preceded by anomalously warm and dry conditions, generating a soil moisture deficit. For European heat waves, other mechanisms, for example involving local SST, are believed to be of less relevance, although some controversy remains (Della-Marta et al. 2007; Duchez et al. 2016; Wehrli et al. 2019).

The Mediterranean region is often referred to as a hotspot of climate change due to a substantial amplification of global warming, especially in summer (Fischer and Schär 2010; Barcikowska et al. 2020). The amplification can partly be explained by a substantial decrease in soil moisture availability. In future warmer climates, this lack of soil moisture—and hence the amplification—is expected to propagate northward, impacting central Europe (Vogel et al. 2017; Suarez-Gutierrez et al. 2020; Wehrli et al. 2020). Overall, it is now well established that climate change has made heat waves more frequent, intense, and prolonged (Chapman et al. 2019; Perkins-Kirkpatrick and Lewis 2020; Sánchez-Benítez et al. 2020); and this trend is expected to continue in the future (Schoetter et al. 2015; Junk et al. 2019; Suarez-Gutierrez et al. 2020).

Climate models and observations have been used to quantify how the odds of extreme temperatures that occurred during specific heat waves have changed from the past and how much they will change in the future (e.g., Vogel et al. 2019; Zhou et al. 2019; Vautard et al. 2020). For example, an event like the July 2019 heat wave in France or Germany is now considered to be at least 10 or 3 times, respectively, more likely to occur than in 1900 (Vautard et al. 2020), and such an extreme event will be ~150 times as probable by the end of the century for the SSP585 scenario (i.e., a 1.8- vs 273-yr return period by the end of the twenty-first century as compared with 1950–2014; Ma et al. 2020). Despite some obvious successes of this *probabilistic approach*, as argued by Shepherd (2016), it has some limitations. First, projected

changes of the polar jet stream in a warmer climate are still highly uncertain (e.g., Shepherd 2014; Hoskins and Woollings 2015; Woollings et al. 2018). Hence, large ensembles are needed to provide meaningful statements. Furthermore, it is rather difficult to find good future analogs of heat waves, not least given that in terms of impacts (e.g., on hydrology) the temporal evolution of the system prior to the heat wave is critical as well. Second, the probabilistic approach does not make the anticipated changes in a warming world readily accessible to the general public and some decision-makers; this is in stark contrast to so-called storyline scenarios (explored in this study) where the impact of climate change is illustrated by considering recent extreme events that people have experienced and can connect to (Shepherd et al. 2018).

The storyline approach provides a way to disentangle dynamic from thermodynamic changes and has been explored in several recent studies (Schubert-Frisius et al. 2017; Shepherd et al. 2018; Wehrli et al. 2020; Van Garderen et al. 2021). In contrast to possible dynamic changes (e.g., meandering of the jet stream), thermodynamic changes associated with heat waves in a warmer world are better understood and associated with relatively small uncertainty (Cattiaux et al. 2015; IPCC 2018; Fan et al. 2020). Increasing CO₂ concentrations, for example, are known to warm near-surface temperatures globally, and warmer SSTs lead to enhanced warm-air advection to downstream land regions (e.g., Dommengat 2009). In the deterministic storyline approach, heat waves are simulated in alternative past and future climates, using an atmospheric general circulation model in which the dynamics in the free troposphere are nudged toward observations using reanalysis data. These simulations start some years before the event to appropriately capture the evolution preceding the events (e.g., spinning up soil hydrology).

So far, two different approaches were used for nudging. In Wehrli et al. (2020) the zonal and meridional winds were nudged; meanwhile, in van Garderen et al. (2021), divergence and vorticity truncated at T20 (spectral nudging) were employed to impose the large-scale dynamical evolution. As both studies used a global climate model, the sea surface temperatures (SST) and sea ice concentration (SIC) had to be prescribed. For the present-day simulations, the observed SST and SIC, including the variability possibly impacting the considered extreme events, were prescribed. For the past and future climate conditions, a climate change signal was added to the SSTs. This is a reasonable approach as it preserves the variability. However, it implies that one needs to rely on the climate change response of a separate, coupled configuration of the same (or similar) atmosphere model, as in van Garderen et al. (2021), or on the response of one or more completely different climate models, as in Wehrli et al. (2020). The atmosphere-only storyline approach also assumes that the impact of a specific extreme event on the ocean state remains the same in different climates, neglecting possible nonlinearities. Moreover, prescribing SIC poses a particular challenge because the simple addition of a local climate change signal can lead to unphysical values and, more fundamentally, is not suited for the way sea ice responds to climate change by spatial migration of the ice edge rather than locally

continuous changes. Wehrli et al. (2020) addressed this with a rather complex approach, whereas van Garderen et al. (2021) neglected SIC changes altogether, after having verified through sensitivity tests though that their influence on the 2010 Russian heat wave is negligible. In fact, given that their focus is on European heat waves, details on how sea ice is treated may not influence their conclusions.

The potential of the uncoupled storyline approach in capturing extreme events such as the European heat waves of 2003 and 2018 along with the Russian heat wave of 2010 has been demonstrated by Wehrli et al. (2020) and van Garderen et al. (2021). It has been shown, for example, that the fraction of the “AgPop” region [i.e., latitudes north of 30°N with a population density above 30 km⁻² or important for agriculture, as defined by Seneviratne et al. (2018)] experiencing daily maximum temperatures higher than 40°C in an event like the 2018 heat wave would quadruple in a future 4-K-warmer climate (Wehrli et al. 2020). Van Garderen et al. (2021) found robust warming from the preindustrial period to the present day for the 2003 and 2010 heat waves, with local warming of about 0°–2.5°C (2003) and 0°–4°C (2010). In both studies, when the warming is averaged for the heat-wave region, an amplified warming (relative to the global-mean warming) is found, except for the 2003 heat wave.

The purpose of this work is to further explore and extend the storyline approach using spectral nudging in a coupled model for answering three central questions: First, how would the 2019 European summer and particularly the July heat wave have developed in preindustrial times? Second, how might they unfold in future warmer climates (+2 and +4 K)? And third, is the coupled storyline approach capable of constraining the surface-ocean and sea ice states? To this end, we have run experiments with the Alfred Wegener Institute coupled climate model AWI-CM-1.1-MR (Semmler et al. 2020) with the large-scale atmospheric circulation in the free troposphere being nudged to reanalysis data, while allowing thermodynamic and small-scale dynamical processes to develop relatively freely. Unlike in related previous studies mentioned above, a fully coupled climate model is used that contributed to phase 6 of the Coupled Model Intercomparison Project (CMIP6; Eyring et al. 2016). By branching the nudging experiments off certain states from the CMIP6 trajectories (e.g., 2-K-warmer climate), plausible states for the sea ice–ocean component of the climate system are readily available and do not need to be explicitly specified like in corresponding atmosphere-only experiments. In section 2, we define the methods used in this work, including the nudging parameters selected. In section 3, the main results are presented. In section 4, the obtained results are briefly discussed, and the main conclusions are highlighted.

2. Methods

Our simulations are based on the Alfred Wegener Institute Climate Model (AWI-CM-1.1-MR; Semmler et al. 2020). This model has contributed to CMIP6 and employs the atmospheric model ECHAM6.3.04p1 from MPI-M (Stevens et al. 2013) coupled to the Finite Element Sea Ice–Ocean Model

(FESOM) v.1.4 (Wang et al. 2014). The atmosphere model is run at T127L95 spectral resolution (~100-km horizontal resolution in the tropics), with 95 vertical levels going up to ~0.01 hPa. The ocean mesh has a variable resolution with refinement in energetically active areas such as the Gulf Stream (Sidorenko et al. 2015; Sein et al. 2017). More specifically, ocean resolution varies from 8 to 80 km, with 8–10 km used in the North Sea, 10–12 km in the Mediterranean Sea, and 8–20 km in the Arctic (Fig. 1 in Semmler et al. 2020).

We have used spectral nudging to impose the observed large-scale circulation for certain atmospheric vertical layers. This technique forces a climate model to follow specific large-scale circulation conditions using reference data from reanalysis (Waldron et al. 1996; von Storch et al. 2000; Zhang et al. 2014). Spectral nudging is implemented by adding an additional nudging term to the model’s governing equations

$$\frac{\partial X_n^m(\eta, t)}{\partial t} = F_n^m(\eta, t) + G_n^m(\eta) [X_n^{m(\text{reana})}(\eta, t) - X_n^m(\eta, t)], \quad (1)$$

where m and n are the zonal and total wavenumbers, respectively; $X_n^m(\eta, t)$ and $X_n^{m(\text{reana})}(\eta, t)$ represent the spectral coefficient of a meteorological variable at the vertical level η and time step t and the same thing from the reanalysis, respectively; $F_n^m(\eta, t)$ denotes the model forcing; and $G_n^m(\eta)$ represents the nudging coefficient.

The impact of nudging depends on which meteorological variables, wavenumbers, and vertical levels are constrained. In this work, only divergence and vorticity are nudged. Hence, all other variables can be freely determined by the model. For our main experiments we use a T20 triangular truncation (i.e., wavenumbers for vorticity and divergence up to 20 are retained); higher-wavenumber dynamics corresponding to smaller spatial scales can be freely computed by the model. T20 was chosen since this is the lowest total wavenumber for which we found the jet stream (winds at 250 hPa) from ERA5 data (Hersbach et al. 2020) to be qualitatively and quantitatively well constrained (an example is shown in Fig. S1 in the online supplemental material) when compared with the full field. Furthermore, we chose to only nudge model levels between 100 and 700 hPa. Sensitivity experiments with different vertical profiles of the nudging coefficient have shown that the influence of additionally constraining the stratosphere or lower troposphere is negligible (Fig. S2 in the online supplemental material). To avoid overfitting and to allow the boundary layer to respond freely, therefore, model levels above 100 and below 700 hPa were not nudged in our simulations.

Similar to previous studies (Schubert-Frisius et al. 2017; Wehrli et al. 2018; Van Garderen et al. 2021), a constant nudging strength is used for the constrained levels. To avoid an abrupt transition between neighboring levels, however, the vertical nudging profile has also been smoothed using a sigmoid function (Fig. S3 in the online supplemental material). The nudging strength is related to an e -folding time τ , with the latter being the inverse of the former (i.e., the larger the e -folding time is, the weaker is the nudging effect). It turns

out that an e -folding time of 24 h provides a good balance between constraining the large-scale atmospheric circulation and allowing differences depending on the boundary conditions to emerge. Figure S4 in the online supplemental material shows 850-hPa winds on one randomly selected day (18 July 2018) from experiments with e -folding times of 6, 24, and 48 h. Results are almost indistinguishable between 6 and 24 h, with some differences emerging if an e -folding time of 48 h is used. Hence, 24 h appears to be a good compromise between imposing the observed atmospheric flow onto the coupled climate model and providing the model with a maximum of freedom to simulate relevant processes and feedbacks, at least for midlatitude heat waves considered in this study.

With this configuration, we have run nudged storyline experiments using atmospheric forcing fields for the period from 1 January 2017 to 30 September 2019. More specifically, nudging experiments with AWI-CM have been branched off the corresponding historical CMIP runs (Semmler et al. 2018) on 1 January 1851 to give *preindustrial* climate conditions, *present-day* conditions were obtained by branching off the Shared Socioeconomic Pathway scenario ssp370 (Semmler et al. 2019) on 1 January 2017, and 2- and 4-K-warmer climates were explored by branching off the ssp370 scenario using as starting point model states when these warming targets are reached (computed applying an 11-yr centered moving average) for all ensemble members (i.e., on 1 January 2038 and 1 January 2093, respectively). For each of the different time slices, we have run five ensemble members starting from the five respective CMIP6 ensemble members.

The nudged simulations started from different ensemble members of the free-running climate model with different initial states for the atmosphere and ocean. Among others, this allows us to quantify how the different ensemble members adjust to the imposed observed forcing. Figure 1 shows the temporal evolution of the ensemble spread of European maximum t2m (computed as the difference between the maximum and minimum of all ensemble members for each day) for the nudging experiment under present-day conditions (similar results are obtained for other boundary conditions or variables; not shown). The ensemble spread is larger than 10 K at the beginning of the simulations; however, it reduces to about 1.5 K within the first few months, suggesting that the first few months should be discarded from the analysis for atmospheric fields. Nevertheless, we allow for one year of spinup time to reach a stabilization for more slowly responding parameters such as soil moisture, sea ice concentration, and SST. Accordingly, where not stated otherwise, simulations with the large-scale dynamical conditions for the period from 1 January 2018 to 30 September 2019 prescribed for preindustrial, present-day, and both 2- and 4-K-warmer climates are analyzed.

Similar to previous studies (e.g., Takhsha et al. 2018; Wehrli et al. 2019), we have found that the global model climatology is not strongly affected by the nudging, with differences lying within the ensemble spread (see, e.g., global and European mean temperature differences among the experiments in Fig. S5 in the online supplemental material). While this holds for the relatively short nudged simulations that are analyzed

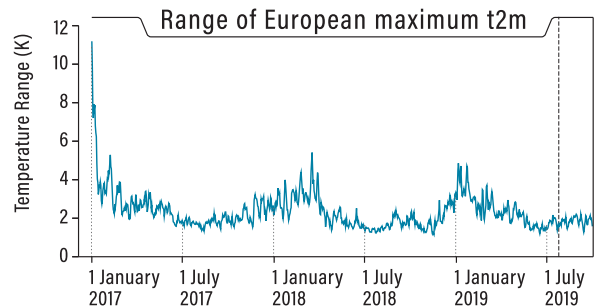


FIG. 1. Temporal evolution of the range of daily maximum t2m for Europe (see Fig. S7d in the online supplemental material for more details on the region). The range is computed as the difference between the daily maximum and minimum values of the five ensemble members for each day. Larger values indicate that maximum t2m is less well constrained by the nudging. The peak of the European heat wave on 25 Jul 2019 is marked by the vertical dashed line.

here, it is possible that the coupled-model climate is significantly and detectably modified—by the changed wind climatology, by numerical effects associated with the nudging per se, or by both—if the nudging is conducted over longer time periods, which should be assessed in future research. Therefore, due to the limited length of the nudged simulations, the five free runs with AWI-CM-1-1-MR from the CMIP6 archive have been used to compute climatologies. To determine anomalies, the period 1981–2010 was used as a reference (except for sea ice, for which 2007–16 period was selected due to the strong sea ice decline of the last decades); meanwhile when the different climates were compared an 11-yr centered moving window was chosen.

3. Results

a. Assessment of the nudged simulations for Europe under present-day conditions

Before discussing the storyline scenarios, we compare the present-day nudged simulations with ERA5. Here we focus on Europe; section 3c provides an assessment for Arctic sea ice.

An example for nudged simulations in comparison with ERA5 data is given for 25 July 2019 (peak of the heat wave; Fig. 2) before we turn to a quantitative analysis. The anomalous circulation in the coupled climate model on that day, expressed in terms of 500-hPa geopotential height (Z500), is an excellent analog of the observed blocking conditions. The same is true for parameters such as temperature at 850 hPa (T850) and maximum t2m anomalies, which are not directly constrained by the spectral nudging. Overall, the observed characteristics of the heat wave over northwestern Europe are thus well captured. As discussed in more detail below, there is evidence that maximum t2m are slightly underestimated in some regions impacted by the heat wave (Figs. 2e,f). Anomalies of SST and soil moisture at level 1 (SML1) associated with this extreme event are also well captured, confirming that climate anomalies associated with central European

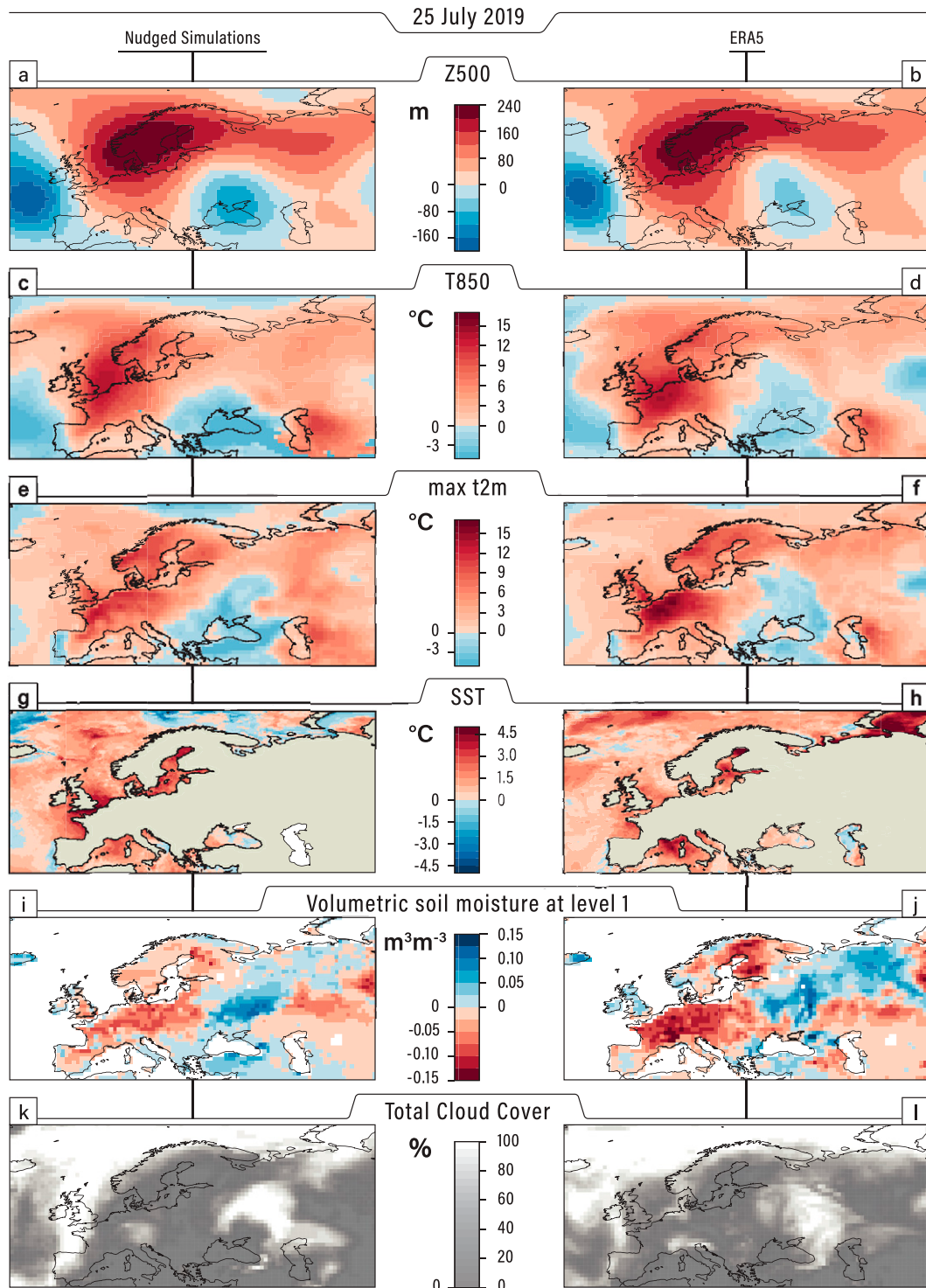


FIG. 2. Anomalies from (left) the nudged present-day simulations and (right) ERA5 for 25 Jul 2019 and different variables: (a),(b) 500-hPa geopotential height; (c),(d) 850-hPa temperature; (e),(f) maximum 2-m temperature; (g),(h) sea surface temperature; and (i),(j) volumetric soil moisture in the first layer. Anomalies were computed as the differences of daily value from the 15-day moving average in the 1981–2010 period. Also shown is total cloud cover on 25 Jul 2019 for (k) the nudged present-day simulations and (l) ERA5.

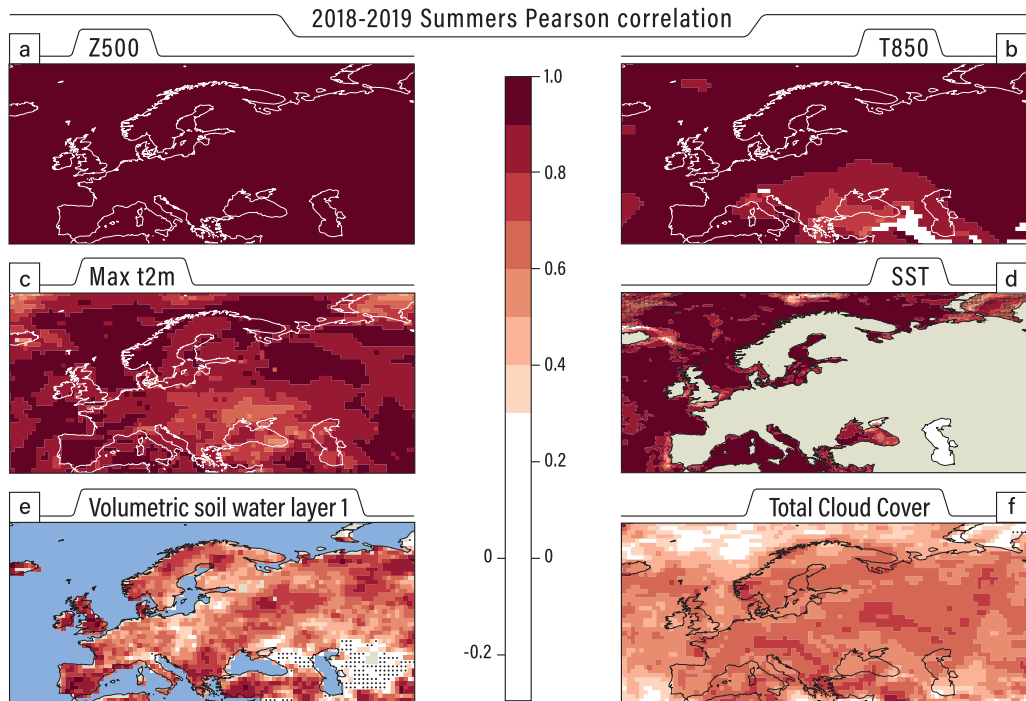


FIG. 3. Pearson correlation between present-day simulations and ERA5 for the summers of 2018 and 2019 using daily fields: (a) 500-hPa geopotential height, (b) 850-hPa temperature, (c) maximum 2-m temperature, (d) sea surface temperature, (e) volumetric soil moisture in the first layer, and (f) total cloud cover. Grid points with nonsignificant correlation ($p > 0.05$) computed using the probability density function of the sample are stippled.

heat waves are strongly driven by atmospheric circulation anomalies. Negative anomalies of SML1 are also slightly underestimated in our nudging experiments, which could partly explain the findings for maximum t2m. Even fields such as total cloud cover (TCC) are reasonably well captured in the Euro-Atlantic region by the nudged simulations for present-day conditions (Figs. 2k,l), suggesting that the cloud physical processes are not negatively influenced by the nudging of vorticity and divergence.

There are some mismatches between the storyline simulations and ERA5 for this particular day (e.g., in the Balkans, central Iberia, and some Arctic regions); note, however, that for parameters such as TCC or SML1 the reanalysis itself is not necessarily well constrained by direct observations. Overall, our results give confidence that the storyline setup with the coupled model captures key processes related to European heat waves—including atmospheric blocking, warm-air advection, clear skies, and soil moisture deficits—if driven by large-scale wind fields from ERA5 in the free troposphere.

So far, our assessment has focused on one particular day at the peak of the July 2019 heat wave. For a more comprehensive assessment, correlations between our storyline simulations for present-day conditions and ERA5 as a proxy for observations for the summers of 2018 and 2019 are shown in Fig. 3. Sizeable correlations are obtained for critical variables that are not nudged in our simulations. We have repeated the

correlation analysis after having removed low-frequency variability, including the seasonal cycle (i.e., removing a 15-day running mean prior to the analysis). Even for high-pass-filtered data, correlations remain high, with values exceeding 0.6 for all parameters except soil moisture, which is probably more influenced by local convective processes (Fig. S6 in the online supplemental material). In summary, therefore, our method not only works well for single extreme cases but, more generally, also captures daily-to-seasonal variability in Europe during summertime.

This point is further illustrated by Fig. 4, which shows the simulated and reanalyzed maximum, minimum and mean t2m time series for Europe and Germany for the period 1 June to 31 August 2019 (see the definition of these areas in Fig. S7 in the online supplemental material). For both regions, the nudged simulations capture the variability very well. In fact, correlations between simulated and reanalyzed time series mostly exceed $r = 0.9$. For Europe, however, some differences emerge on longer seasonal time scales: Although the climate model tends to slightly underestimate t2m in early June, during the course of the summer positive t2m biases emerge. Further analysis suggests that there are small pan-European cold biases in early summer, turning into larger warm biases in southeastern Europe from late June (Fig. S8 in the online supplemental material). The time series for Germany (Fig. 4) generally indicates smaller maximum t2m biases for the coupled model. However, there is

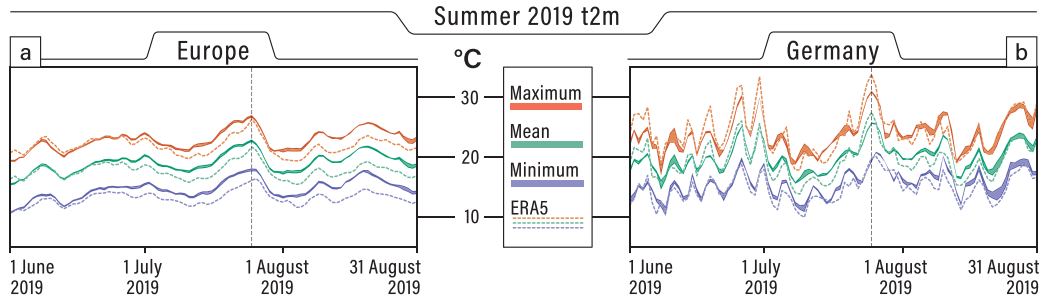


FIG. 4. Seasonal evolution of daily minimum (purple), daily mean (green), and daily maximum (orange) 2-m temperature for (a) Europe and (b) Germany and the period from 1 Jun to 31 Aug 2019. Results are shown for the nudged simulations under present-day conditions (shading) as well as for ERA5 reanalysis data (dashed lines). Shading denotes the minimum/maximum range of values obtained from the respective five-member ensembles. The peak of the European heat wave on 25 Jul 2019 is marked by the vertical dashed line.

some evidence for the exceptionally warm periods in June and July 2019 to be underestimated, especially for maximum t_{2m} during daytime. On the other hand, the coupled model simulates realistic t_{2m} for the third heat wave in late August 2019. Our analysis suggests that the biases are flow dependent; the circulation patterns are different, with an exceptional subtropical ridge prompting the June 2019 heat wave, whereas the July and August events are associated with a blocking located in different sectors (European west, from

0° to 15° E, and European east, from 15° to 30° E; Sousa et al. 2018). In this context, it can be argued that the spectral nudging approach—like more sophisticated data assimilation methods such as 4D-Var (e.g., Rodwell and Palmer 2007)—has strong diagnostic potential to help unravel the causes of biases in coupled climate models at the process level, thus guiding model development.

To further explore the flow dependence of the t_{2m} biases for Germany, we have selected the 10 days with the strongest

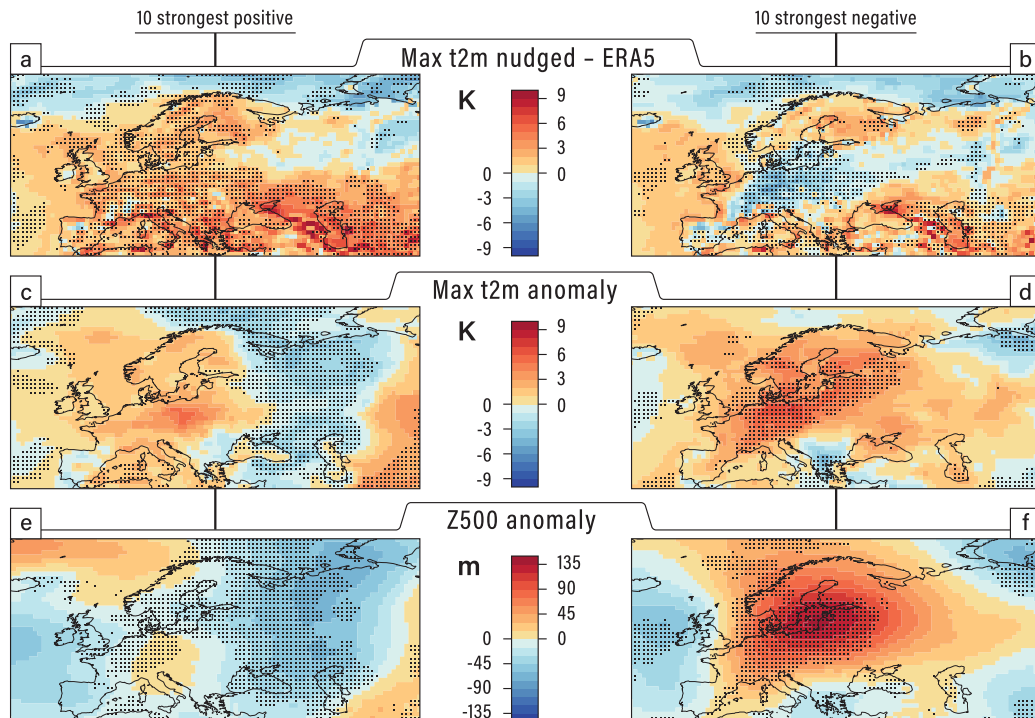


FIG. 5. (a),(b) Maximum t_{2m} differences between the nudged present-day simulations and ERA5, (c),(d) maximum t_{2m} anomaly, and (e),(f) Z500 anomaly for the 10 days with the strongest (left) positive and (right) negative Germany maximum t_{2m} differences between the simulations and ERA5. The summers of 2018 and 2019 were included. Grid points at which the differences are significant ($p < 0.05$) computed using a Mann-Whitney U test are stippled.

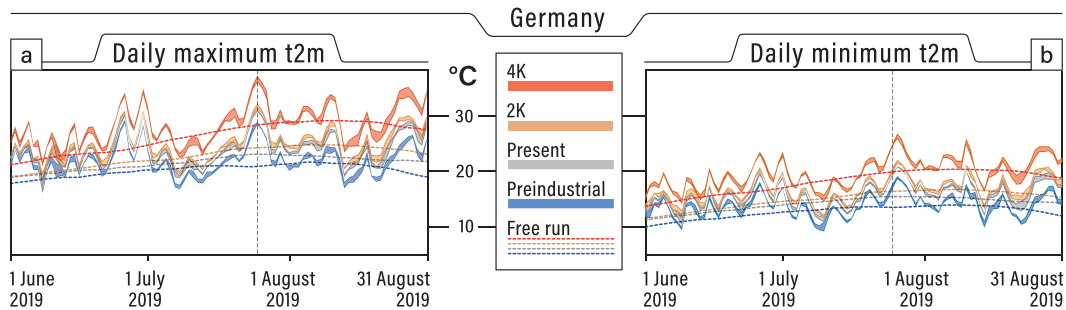


FIG. 6. Seasonal evolution of daily (a) maximum and (b) minimum t_{2m} averaged for Germany and different climates (preindustrial in blue, present-day in gray, +2 K in orange, and +4 K in red). Shading spans the minimum/maximum range of values obtained from the five-member ensembles, and dashed lines show the mean from the free run. Differences are shown in Fig. S9 in the online supplemental material. The peak of the European heat wave on 25 July 2019 is marked by the vertical dashed line.

positive and strongest negative max t_{2m} differences for Germany between our nudged simulations and ERA5 (Fig. 5), using summer data from 2018 and 2019 (see Table S1 in the online supplemental material). The most striking finding from this analysis is that the climate model tends to underestimate the maximum t_{2m} during heat waves in Germany, which are governed by the presence of a pronounced anomalous anticyclonic circulation anomaly, and thus strong European blocking events. No such coherent atmospheric circulation anomaly is found for periods when the simulated t_{2m} in Germany are warmer than in the reanalysis (Figs. 5a,c,e). The finding that the nudged model underestimates extreme t_{2m} during heat waves in Germany is important, especially when it comes to making quantitative statements on the impact of heat waves and their future changes.

b. Storyline scenarios for the European summer of 2019

Having demonstrated that the spectral nudging approach with the coupled climate model works well, we now analyze how the summer of 2019, including the July heat wave, might have evolved in preindustrial times and how it might unfold in future 2- and 4-K-warmer climates. For Germany, there is very robust warming for maximum and minimum t_{2m} (i.e., the ensembles for different climates do not overlap) that tends to grow throughout the summer season, both from preindustrial times to the present and from present-day to 4-K-warmer climates (Fig. 6). Changes in maximum and minimum t_{2m} from present-day conditions (approximately +1.2 K in the storyline experiments) to a 2-K-warmer climate are smaller, even though they are still quite robust in terms of the separation of the two ensembles. In general, these findings are consistent with the free-running CMIP6 simulations (dashed lines in Fig. 6), suggesting that they are not a particular feature of this specific summer.

Another point illustrated by Fig. 6 is that at nighttime t_{2m} (minimum t_{2m}) in Germany in a 4-K-warmer world are projected to become comparable to typical daytime maxima (maximum t_{2m}) in preindustrial times, at least for the heat waves that occurred in late July and August 2019.

Remarkably, this anthropogenic warming in Germany has an intraseasonal cycle (see Fig. S9 in the online supplemental material for maximum t_{2m} , with similar results for minimum t_{2m} , which are not shown), with values close to the global average in early summer and then increasing relative to global value in mid- and late summer. In fact, values around +5.5 K (+4 K minus present-day), +0.8 K (+2 K minus present-day), and +2.0 K (present-day minus preindustrial) are obtained for the July heat wave peak. Hence, there is evidence for global warming amplification in phase with the July event, particularly in the 4-K-warmer climate (a twofold increase). Similar results can be found in the free run as well as in observational data (DWD 2021), so this amplification is not specific to the events in July 2019. When the differences are computed for +2 K minus preindustrial and +4 K minus +2 K, and then nonsignificantly higher warming is obtained for the latter (supplemental Fig. S9, bottom). This suggests that there might be some feedback mechanisms generating a slightly higher than expected warming in the future.

The European heat waves during the summer of 2019 did not only impact land areas; they were also accompanied by ocean heat waves in the North Sea, as demonstrated in Fig. 7, which shows the evolution of SST in the North Sea and the German Bight (see their definition in Fig. S7 in the online supplemental material). In general, the ocean heat waves are more pronounced for the latter region (especially for late June and August events). This is not too surprising given that it represents a smaller and shallow area that lies closer to the area most impacted by the heat waves. Around mid-July, SST in the German Bight is about 1 K cooler in the nudged runs relative to the climatological signal derived from the free runs; shortly before 25 July, anomalies turn positive, reaching about +2 K in late July and early August. Thus, the impact of heat waves on SST in both areas suggests that using coupled climate models for storyline scenarios may be an advantage when it comes to capturing events that are impacted by coupled processes.

From a climatological point of view, the warming of SST in the German Bight from preindustrial times to the 4-K-warmer world amounts to about 4 K. This is a substantial change in

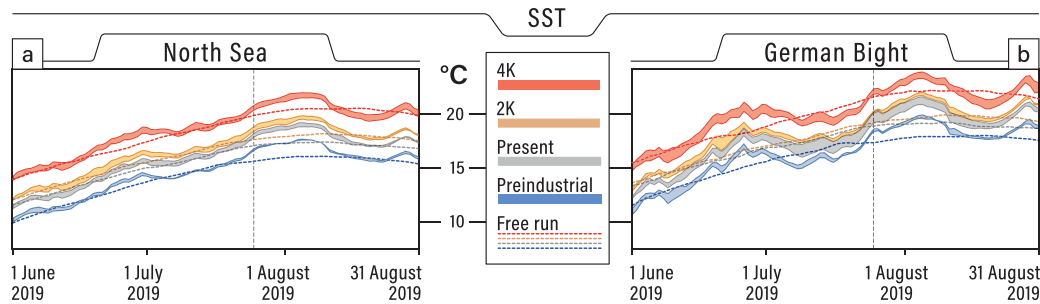


FIG. 7. As in Fig. 6, but for sea surface temperature in (a) the North Sea and (b) the German Bight.

comparison with SST changes in the open ocean (~ 3 K). The ocean heat wave in early August, for example, would have been accompanied by SSTs of about 19° – 20° C in preindustrial times; in a 4-K-warmer world, SSTs could reach up to 24° C. The change is probably even larger in the shallow waters closer to the coast not resolved by the climate model (~ 8 km is used in the North Sea). Furthermore, it is worth pointing out that, relative to t2m, for SST changes there is even less evidence for a warming acceleration when comparing the warming from +2 to +4 K with the warming from

preindustrial times to +2 K (Fig. S10 in the online supplemental material). This is consistent with an earlier finding that the observed warming in the North Sea during the last few decades was quite strong (Wiltshire et al. 2010).

The evolution of SST warming in the nudged 2019 storyline simulations exhibits some interesting differences when compared with the corresponding climatological warming. For example, considering the change from present-day to the 4-K-warmer climate, SSTs in the German Bight increase by about 0.5–1 K more in the storyline runs in June 2019 than in the climatological warming, whereas the opposite holds for August 2019 (Fig. S10 in the online supplemental material), resulting in an increased strength of the June heat waves and a dampened strength of the late summer heat waves (Fig. 7). Even though a robust detection of this effect with the five-member ensemble is difficult (complete separation of the ensemble from the free-run value corresponds to a p value of 0.0625 according to a two-sided Wilcoxon signed rank test), this provides evidence for a dependence of the SST climate-change signal on weather patterns that could not be captured by storyline scenarios using atmospheric models with prescribed SSTs.

Spatial maps of the t2m differences on 25 July 2019 between the different climates for the wider European region are shown in Fig. 8. These maps describe the “warming signal of the day,” given the large-scale circulation and its evolution during the preceding days, weeks and months. Some well-known climate change features (e.g., Fischer and Schär 2010; Barcikowska et al. 2020; Suarez-Gutierrez et al. 2020) emerge for this particular day: For example, extreme temperatures over land areas tend to increase more strongly than those over the ocean; the warming is more pronounced in southern Europe relative to more northern regions of continental Europe; and the warming signal tends to move northward during the twenty-first century. Furthermore, anomalously strong warming signals can be found locally in some of the regions (e.g., northeastern Spain and southwestern France with up to 10 K for the difference between 4-K-warmer and present-day climates), which supports the notion that there may be some “weather-dependent amplification” of climate change. However, not all of the small-scale structures may be due to this weather dependence. Some of the differences may simply be “random,” for example depending on the presence of clouds (less well constrained and thus more uncertain) and hence the strength of the incoming solar radiation.

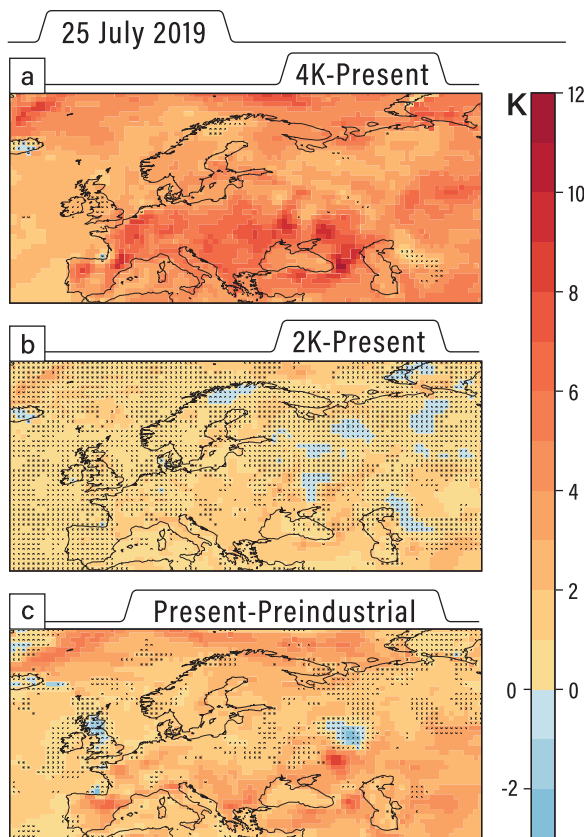


FIG. 8. Daily maximum t2m differences on 25 Jul 2019: (a) +4 K minus present-day, (b) +2 K minus present-day, and (c) present-day minus preindustrial. Locations where the ensembles overlap between different climates are stippled.

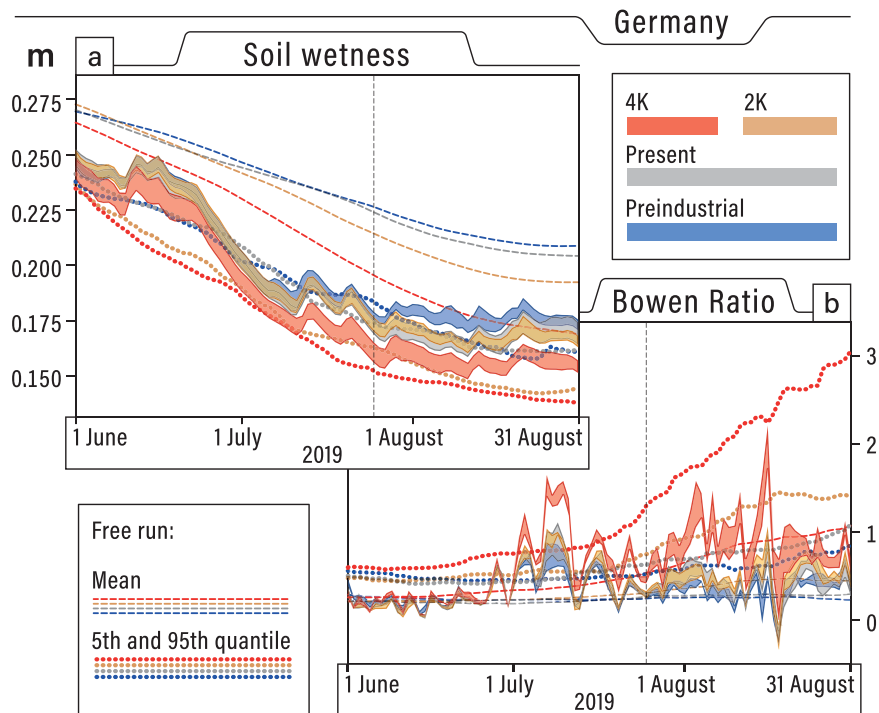


FIG. 9. Seasonal evolution of (a) soil wetness and (b) Bowen ratio in Germany between 1 Jun and 31 Aug 2019 in different climates (preindustrial in blue, present-day in yellow, and 2- and 4-K-warmer worlds in orange and red, respectively). Shading spans the minimum/maximum range of values obtained by the respective five-member ensembles. Dashed lines show the mean, and dotted lines show the 5th and 95th quantile for soil wetness and Bowen ratio climatology, respectively. The peak of the European heat wave on 25 Jul 2019 is marked by the vertical dashed line.

From Fig. 8 it can also be inferred that for some regions in Germany the additional warming from present-day conditions to the end of the twenty-first century (4-K-warmer world) would amount to as much as 7 K. By adding the 3.6 K experienced today as compared with preindustrial times, locally maximum t_{2m} by the end of the century could exceed 47°C ; in contrast, maximum t_{2m} would have stayed below 37°C in preindustrial times—certainly extreme, but not necessarily dangerously high (see Fig. 15 below). Moreover, in the +2-K world, the signal-to-noise ratio of changes relative to the present climate for the heat-wave peak is small so that the present-day and +2-K ensembles overlap almost everywhere (Fig. 8b).

We have also explored the connection between changes in t_{2m} , soil wetness, and Bowen ratio, which is defined as the ratio of sensible to latent heat fluxes. The seasonal evolution of soil wetness and the Bowen ratio in the different climates is shown in Fig. 9. The summer of 2019 starts with anomalously dry soils that were comparable for the different climates (i.e., the ensembles show some overlap). Furthermore, latent heat flux dominates over sensible heat flux in June, as indicated by the Bowen ratios remaining below 0.5 for all climates. Driven by the first heat wave in late June 2019 (Fig. 6), a dramatic decrease in soil wetness is witnessed in all simulations, with values reaching the 5th quantile obtained from the CMIP6 ensemble (dotted lines in

Fig. 9). The more moderate conditions in early and mid-July led to a minor increase in soil wetness. As a consequence, the July heat wave occurred with anomalously, but not exceptionally dry soils (below the 4-K-warmer climate climatology). In early July, the reduced soil moisture availability triggered an increase in Bowen ratio to values around 1. Nevertheless, after a small decrease in mid-July, the values on the heat-wave peak are only slightly higher than the climatology. This suggests that dry soils exacerbated the July heat wave but were not a key factor.

Remarkably, the consequences of the June event in both variables are even greater in the 4-K-warmer climate, with robustly drier conditions and a higher Bowen ratio from early July to the end of the season. Thus, these higher changes in the radiative fluxes (due to a lack of soil moisture) can partly explain the larger warming amplification observed in this area in the future 4-K-warmer climate. Therefore, a heat wave in early summer (as in 2003 or 2019) could exacerbate a heat wave occurring later (high summer) as it creates dry soil conditions that intensify the second event by changes in the surface heat fluxes. Furthermore, at least for the 2019 summer, this effect would be stronger in the 4-K-warmer climate than in the climates from preindustrial to 2 K warmer.

Maps of soil wetness and Bowen ratio for 25 July 2019 are shown in Fig. 10. They help to explain the global warming amplification and nonlinear changes found for t_{2m} . From the

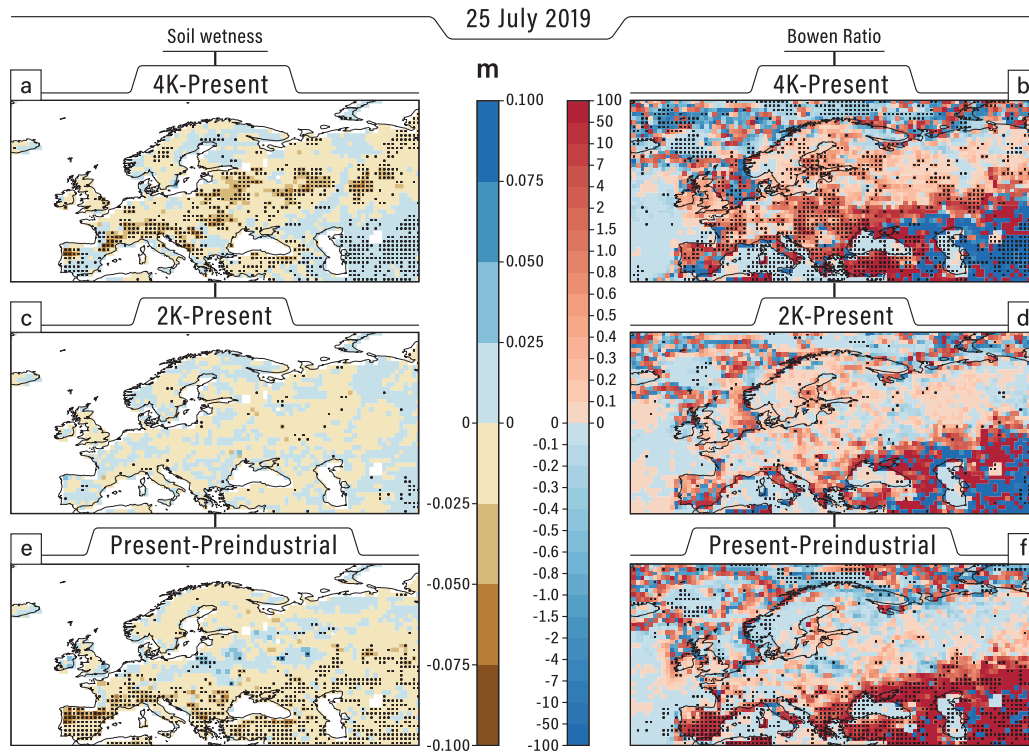


FIG. 10. (left) Soil wetness and (right) Bowen ratio differences between (a),(b) 4 K warmer and present; (c),(d) 2 K warmer and present; and (e),(f) present and preindustrial climates on 25 Jul 2019. Locations where the two ensembles do not overlap are indicated by stippled.

preindustrial to present-day climates, there is a strong and robust drying in the Mediterranean region that is accompanied by a dramatic increase in the Bowen ratio. Meanwhile, in central and northern Europe differences are relatively small due to the availability of sufficient soil moisture. When considering future changes (i.e., +4 K minus present-day) the drying of the soil and the increase in Bowen ratio peak in mid-latitude regions, including central Europe.

c. Storyline scenarios for Arctic sea ice

The use of a coupled model allows studying coupled environmental extreme events, as mentioned in section 3b for SST in the North Sea. Here we provide some initial insight into the value of the coupled storyline scenario approach for Arctic sea ice. In general, studying sea ice anomalies in a coupled storyline approach might be useful not only to explore more directly sea ice–related extremes, such as the opening of polynyas north of Greenland (Moore et al. 2018; Ludwig et al. 2019); sea ice anomalies have also been shown to influence midlatitude events, such as extreme snowfall in northern Europe, through modification of air masses (Bailey et al. 2021). Here we therefore briefly discuss how Arctic sea ice anomalies and changes are represented in our coupled storyline simulations, acknowledging that sea ice probably had a minor role to play when it comes to thermodynamic processes driving European heat waves.

Daily anomalies of the pan-Arctic sea ice extent (area with SIC > 15%) are relatively coherent between the nudged simulation and ERA5 (Fig. 11). Omitting the first year, where the model state might still be affected by the spinup, the Pearson correlation for the ensemble mean is ~ 0.65 (~ 0.53 if the first year is included). While some of the strong anomalies are clearly captured, in particular during the second half of 2018, some anomalies are not well captured by the nudged simulation. In particular, observed negative anomalies around April both in 2018 and 2019 are in contrast to positive anomalies in the storyline simulations. However, it is worth noting that the ensemble spread during these inconsistent periods is much larger than during the second half of 2018, suggesting that the sea ice state may be less strongly constrained by the large-scale circulation in the early melt season than at other times of the year.

Another factor that can lead to inconsistent anomalies is model bias. While this probably holds for any quantity, it may be particularly influential for the sea ice state. Moderate temperature biases, for example, can lead to significant errors in the ice-edge location. As a consequence, the ice-edge location in a biased model will respond differently to the same large-scale circulation anomaly pattern, simply because the ice edge resides in a different place. Indeed, AWI-CM free runs exhibit nonnegligible biases in the ice-edge location (Semmler et al. 2020), and nudging only the large-scale dynamics does not—and is not meant to—rectify thermodynamically induced

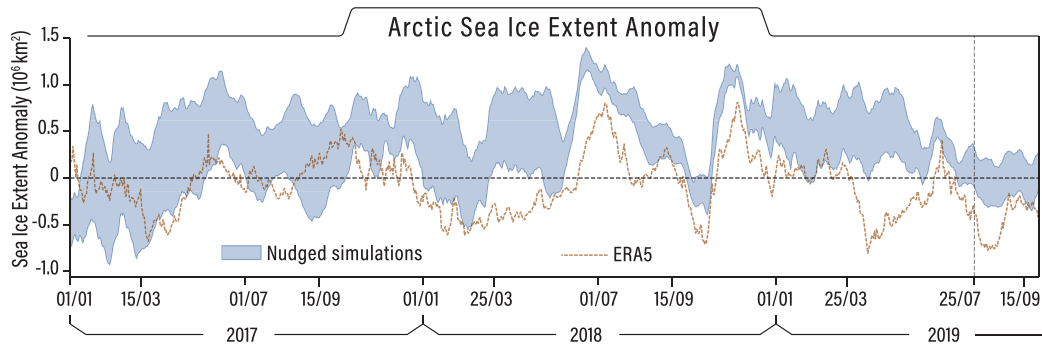


FIG. 11. Arctic sea ice extent anomalies (climatology computed using the 2007–16 period) from ERA5 (dashed line) and the present-day nudged simulation (shading). The peak of the European heat wave on 25 Jul 2019 is marked by the vertical dashed line.

model biases. In July, for example, the climatological ice edge extends much farther into the Barents and Kara Seas in AWI-CM than in ERA5 (black contours in Fig. 12). However, despite these limitations, the regional patterns of sea ice concentration anomalies tend to be captured rather well. For example, during the Arctic melt season 2019 on 25 July (the peak of the central European heat wave), negative SIC anomalies prevailed in the Chukchi, East Siberian, and Laptev Seas, whereas positive anomalies prevailed in (or north of) the Barents and Beaufort Seas (Fig. 12, bottom). While the moderately negative pan-Arctic sea ice extent anomaly at that time is not reproduced (the simulated anomalies are nearly neutral; Fig. 11), the spatial patterns are reasonably well captured (Fig. 12, top).

The fact that the ice edge responds differently to large-scale circulation anomalies depending on where it resides on average is even more important when it comes to sea ice anomalies in significantly different climates: The climatological sea ice distributions in the preindustrial, present, +2-K, and +4-K climates are vastly different (Fig. 13). For example, one

cannot expect that a large-scale circulation pattern that causes, or at least contributes to, a record-low pan-Arctic sea ice extent in preindustrial or present climate would have a similar effect in a 4-K-warmer climate, where scarcely any Arctic sea ice remains even in July (Fig. 13), two months before the end of the classical melt season. This may complicate the assessment to what extent sea ice anomalies associated with a specific extreme event may amplify or dampen some aspects of the event when transferred to a different climate. However, as is the case for SSTs, it is arguably more physically consistent with regard to the two-way interaction of sea ice with an extreme event to simulate the sea ice response in a coupled model rather than to prescribe the sea ice state and its response in some nontrivial way.

4. Discussion and conclusions

In this study we present a method for computing storyline scenarios using spectral nudging in a coupled climate model. The strength of this approach lies in the use of a coupled

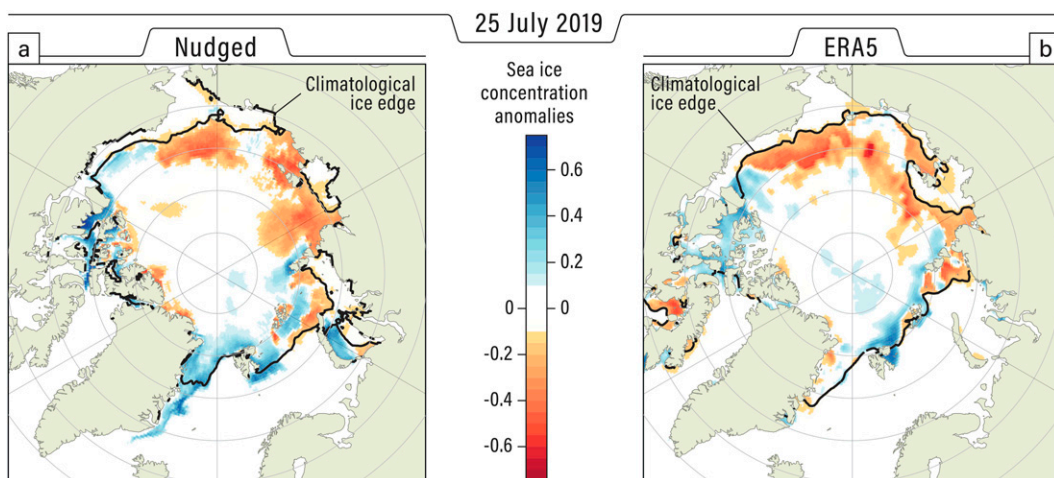


FIG. 12. SIC anomalies (climatology computed using the 2007–16 period) on 25 Jul 2019 from (a) AWI-CM nudged simulations and (b) ERA5. Black contours show the respective climatological 15% sea ice concentration.

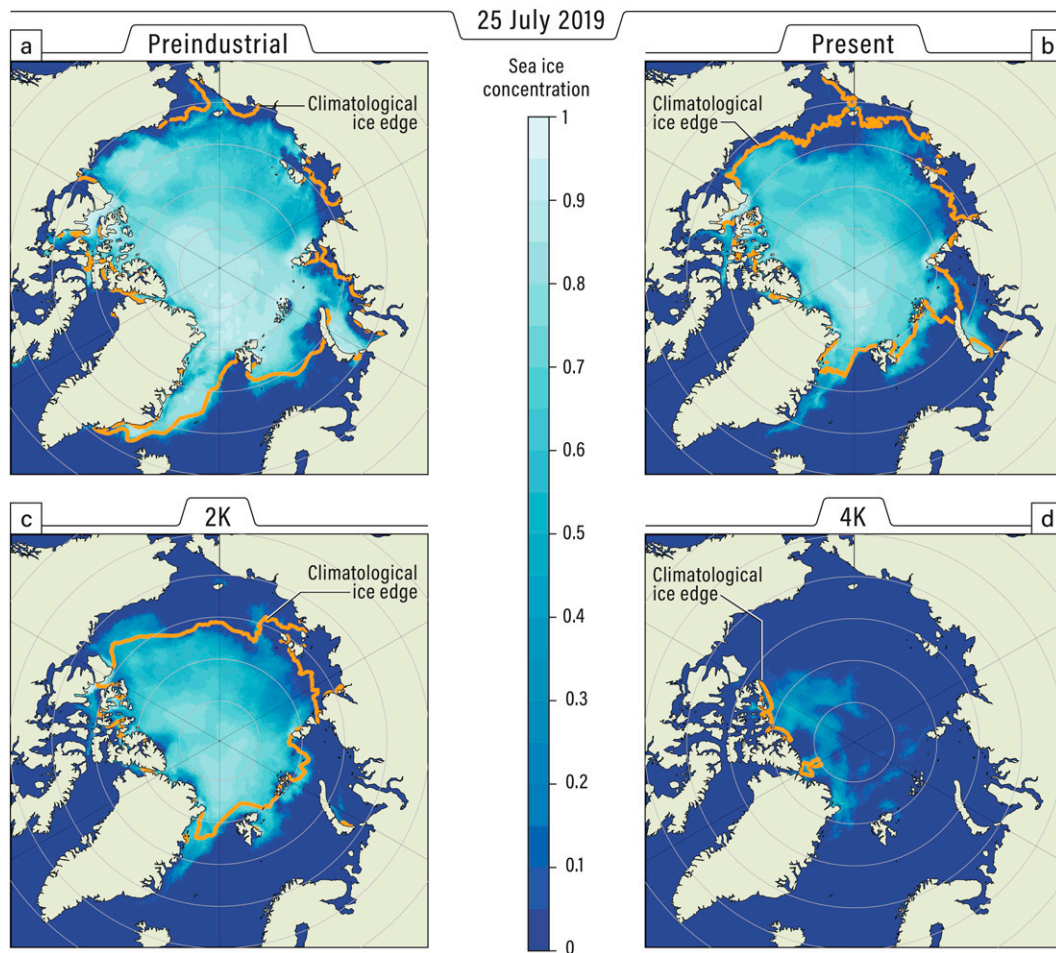


FIG. 13. Sea ice concentration on 25 Jul 2019 from AWI-CM nudging experiments for different climates: (a) preindustrial, (b) present-day, (c) 2-K-warmer world, and (d) 4-K-warmer world. Orange contours show the respective climatological 15% sea ice concentration contour.

climate model that has contributed to CMIP6 (i.e., AWI-CM-1-1-MR; Semmler et al. 2020). By using a coupled approach one can study climate and environmental extremes in a coupled framework, thereby avoiding possible shortcomings that arise from having to specify SST and sea ice conditions for past and future climates. In this context, the availability of CMIP6 simulations, from which the nudging experiments can be branched off, is a distinct advantage. By applying a scale-dependent, spectral nudging approach in the free troposphere only, as in van Garderen et al. (2021), it is possible to constrain only the large-scale circulation associated with the jet stream, which is known to be one of the key drivers of extreme and high-impact environmental events in midlatitudes.

The full potential of this approach can further be inferred from Fig. 14, illustrating coupled storyline scenarios for 1600 UTC 20 September 2019—another event in late summer/early autumn 2019. This confirms that (i) the jet stream (i.e., the dynamic driver) is realistically represented; (ii) anthropogenic warming is strongest over land, especially when considering changes from present-day condition to a 4-K-warmer world;

(iii) locally extreme SSTs anomalies (i.e., ocean heat waves) emerge in the Mediterranean Sea, with SSTs exceeding $+30^{\circ}\text{C}$ in the central Mediterranean Sea; and (iv) there are vastly different sea ice conditions in the Arctic that are consistent with the atmospheric state and its previous evolution. We should note that the last two points are treated in a physically more consistent way in coupled storyline scenarios than it could be by prescribing SST and SIC fields in atmosphere-only storyline scenarios.

The storyline approach, employing nudging, is computationally quite efficient, at least once CMIP-type simulations are available from which nudged simulations can be branched off. This is due to the fact that the main source of uncertainty in future projections of European extreme events—namely, strong internal atmospheric variability as compared with relatively weak climate change signals—has been effectively “removed” by prescribing the temporal evolution of the large-scale midtroposphere dynamics. In fact, in agreement with Wehrli et al. (2020) and van Garderen et al. (2021), for European heat waves just a few ensemble members are

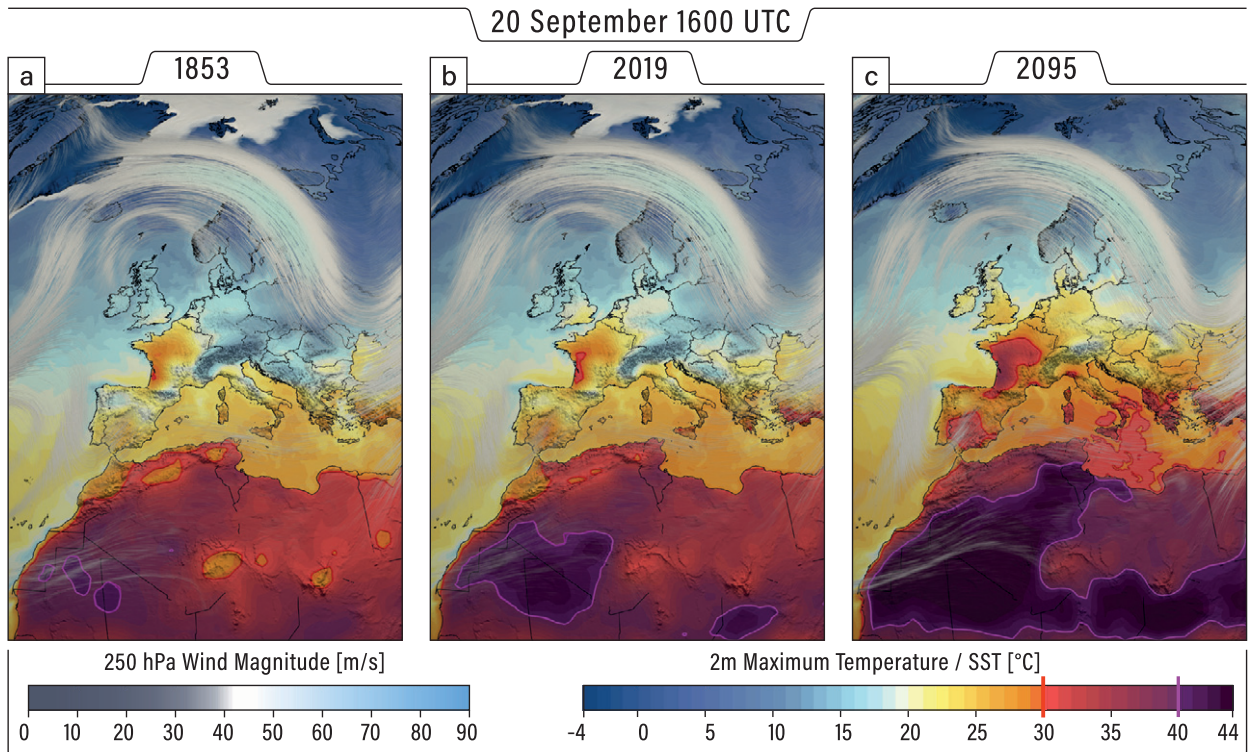


FIG. 14. Storyline simulations of maximum 2-m temperature, sea surface temperature, sea ice, and 250-hPa winds at 1600 UTC 20 Sep 2019 for (a) a preindustrial climate, (b) present-day conditions, and (c) a 4-K-warmer world. The 30° and 40°C isotherms are indicated by thick red and purple contours, respectively.

sufficient to separate signal from noise, once the evolution of the large-scale atmospheric circulation is prescribed.

As pointed out by [Shepherd et al. \(2018\)](#), storyline scenarios provide a very effective way of making the impacts of climate change more tangible to experts and nonexperts alike, thus facilitating decision-making in adaptation and

mitigation. This point is further illustrated in [Fig. 15](#), showing “weather maps” of t2m during the peak of this record-breaking heat wave in Germany in July 2019 for present-day, preindustrial, and future conditions: While this weather event was clearly extreme by nature, with maximum t2m of about 37°C even without anthropogenic warming, the

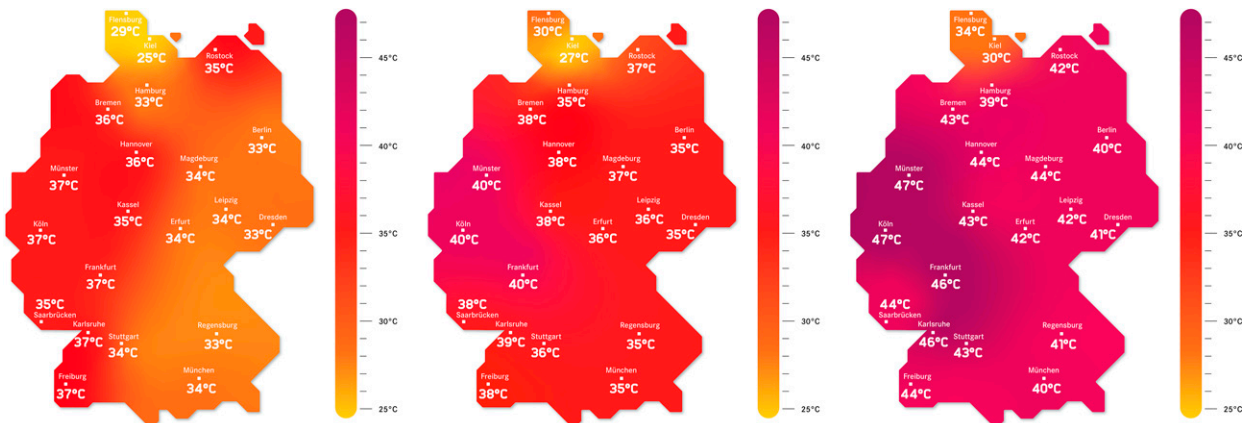


FIG. 15. Schematic maps of 2-m temperature for weather conditions in Germany at 1500 UTC 25 Jul 2019, for (a) a preindustrial climate, (b) present-day conditions, and (c) a 4-K-warmer world. The maps have been produced by graphic designers of the communication team of the Helmholtz Climate Initiative using observed values for the locations shown on the map and by adding temperature increments from the storyline scenarios for preindustrial and 4-K-warmer conditions.

warming since preindustrial times made it record-breaking (42°C in places) with substantial impacts on society, businesses, and infrastructure, including a “meltdown” of the German railway system. In a 4-K-warmer world (i.e., 3 K warmer than today) daytime t2m would be reaching dangerously high values, nearing 50°C . The value of this approach for understanding and communicating the impact of climate change could be further enhanced by using these storyline scenarios to drive impact models. In this way, it would become possible to draw more complete “pictures”—for example, by also making statements about surface hydrology, river levels, and the state of the vegetation.

It seems likely that finding analogs of similar quality from observations, CMIP data, and large ensembles will be difficult, if possible at all. This is especially true if the temporal dimension is taken into account, which is critical when it comes to parameters such as soil moisture and SST that memorize past weather and are not only of interest in their own right but also feed back on temperatures during the evolution of heat waves.

The coupled storyline approach, presented in this study, also provides a very powerful way of diagnosing the origin of model error at the process level, thus guiding future model development. Usually, one of the main challenges in diagnosing coupled models arises from the fact that a direct comparison with observations from field campaigns, which are usually comprehensive and of high quality but limited in time, is difficult to carry out. Therefore, disentangling differences due to different weather from those due to model deficiencies becomes difficult. Recognizing this, activities such as Transpose-CMIP—that is, running short-term predictions with initialized coupled climate models—have been proposed and applied (e.g., van Niekerk et al. 2016; Voldoire et al. 2019). Here we argue that the storyline simulations, using spectral nudging in climate models, provide another promising way of analyzing model shortcomings, including those that occur only sporadically during certain weather types (i.e., flow-dependent biases). To explore this idea further, we are planning to extend the experiments until the end of 2020 and provide a thorough comparison with observational data from the MOSAiC expedition (Multidisciplinary Drifting Observatory for the Study of Arctic Climate; <https://mosaic-expedition.org/>), that is, the year-round drift through the Arctic that lasted from October 2019 to October 2020. Related to this, the approach proposed in this study provides a powerful technique to understand and quantify how coupled processes associated with certain phenomena (e.g., heat waves, sea ice polynyas, and cold-air outbreaks) change in different climates. The fact that dry soils in southern Europe at the end of the twenty-first century in a 4-K-warmer world are projected to change how the atmosphere interacts with the soil is a promising example.

Storyline scenarios are in principle not limited to specific types of events. However, it is likely not a coincidence that studies demonstrating the approach so far have been focusing on heat waves; these have a rather large-scale footprint and can thus be reproduced relatively easily by constraining the large-scale dynamics. While the same may hold for cold extremes in winter, events that occur on smaller scales and involve small-scale dynamics and fronts, including extreme

rainfall events like the devastating flash floods in western Germany in July 2021, are more challenging. In our setup, where the nudging is relatively weak and leaves wavenumbers above 20 free, extreme rains are clearly underestimated (not shown). Dedicated efforts are needed to extend the storyline approach to different types of events. It is possible that different event types will require different optimal settings, and that events with a strong small-scale random component may necessitate a large-ensemble storyline approach.

To summarize, this work presents the first storyline of the European July 2019 heat wave augmenting previous probabilistic attribution studies (Ma et al. 2020; Vautard et al. 2020) in which changes of the frequency of occurrence of certain events in different climates are quantified. The most outstanding finding of this study is the global warming amplification found associated with the July 2019 heat wave (locally up to fourfold increase). This amplification is enhanced and northward displaced in the future 4-K-warmer climate, with more than a twofold increase in Germany (both for maximum and minimum t2m). In contrast with the result obtained by van Garderen et al. (2021) for the European 2003 heat wave, an amplification is also found from preindustrial to present climate (~ 1.5 -fold increase in Germany), with the highest warming found in the Mediterranean region. The warming obtained for the 2019 summer is similar to the climatological mean warming, as may be due to a climatological drying of soils comparable to the drying that occurred during the 2019 summer. In addition, we have not found significant flow-dependent stronger or weaker changes in our simulations (not shown). However, this last result should be assessed using simulations that span longer periods (e.g., starting in 1979). Meanwhile, neither a future global warming amplification nor a summer intraseasonal cycle of warming is found for SST in our study areas (more specifically, the North Sea). However, the observed SST warming there is close to the global warming and thus stronger than the mean ocean-surface warming.

Overall, our study adds further support to the notion that storyline scenarios provide a promising approach that augments traditional probabilistic approaches to the attribution of extreme events and that help to make climate change and its impact more tangible to scientists, decision-makers, and the general public.

Acknowledgments. This work was supported by the Helmholtz-Climate-Initiative through the HI-CAM project (Drivers cluster). Author Goessling acknowledges the financial support by the Federal Ministry of Education and Research of Germany in the framework of SSIP (Grant 01LN1701A). The simulations were performed at the German Climate Computing Center (DKRZ) using the ESM-Tools (Barbi et al. 2021). We thank Sebastian Rast (MPI-M) for support with the spectral nudging in ECHAM, Michael Böttinger (DKRZ) for the visualization in Fig. 14, and the ESM-Tools staff for their assistance during the simulation.

Data availability statement. Data from the AWI-CM-1-1-MR free runs are available in the Earth System Grid

Federation (ESGF) data nodes (e.g., <https://esgf-data.dkrz.de/search/cmip6-dkrz/>; see “Source ID,” etc.). The nudging experiments are stored in the supercomputer Levante from DKRZ and are available online (Zenodo: <https://doi.org/10.5281/zenodo.6348822>). ERA5 reanalysis data used in this study can be accessed from the European Center for Medium-Range Weather Forecasts (ECMWF; <https://www.ecmwf.int/en/forecasts/datasets/reanalysis-datasets/era5>).

REFERENCES

- Bador, M., L. Terray, J. Boé, S. Somot, A. Alias, A. L. Gibelin, and B. Dubuisson, 2017: Future summer mega-heatwave and record-breaking temperatures in a warmer France climate. *Environ. Res. Lett.*, **12**, 074025, <https://doi.org/10.1088/1748-9326/aa751c>.
- Bailey, H., A. Hubbard, E. S. Klein, K.-R. Mustonen, P. D. Akers, H. Marttila, and J. M. Welker, 2021: Arctic sea-ice loss fuels extreme European snowfall. *Nat. Geosci.*, **14**, 283–288, <https://doi.org/10.1038/s41561-021-00719-y>.
- Barbi, D., N. Wieters, P. Gierz, M. Andrés-Martínez, D. Ural, F. Chegini, S. Khosravi, and L. Cristini, 2021: ESM-Tools version 5.0: A modular infrastructure for stand-alone and coupled Earth system modelling (ESM). *Geosci. Model Dev.*, **14**, 4051–4067, <https://doi.org/10.5194/gmd-14-4051-2021>.
- Barcikowska, M. J., S. B. Kapnick, L. Krishnamurty, S. Russo, A. Cherchi, and C. K. Folland, 2020: Changes in the future summer Mediterranean climate: Contribution of teleconnections and local factors. *Earth Syst. Dyn.*, **11**, 161–181, <https://doi.org/10.5194/esd-11-161-2020>.
- Barriopedro, D., E. M. Fischer, J. Luterbacher, R. M. Trigo, and R. García-Herrera, 2011: The hot summer of 2010: Redrawing the temperature record map of Europe. *Science*, **332**, 220–224, <https://doi.org/10.1126/science.1201224>.
- Beilouin, D., B. Schauburger, A. Bastos, P. Ciais, and D. Makowski, 2020: Impact of extreme weather conditions on European crop production in 2018. *Philos. Trans. Roy. Soc. London*, **B375**, 20190510, <https://doi.org/10.1098/rstb.2019.0510>.
- Cattiaux, J., H. Douville, R. Schoetter, S. Parey, and P. Yiou, 2015: Projected increase in diurnal and interdiurnal variations of European summer temperatures. *Geophys. Res. Lett.*, **42**, 899–907, <https://doi.org/10.1002/2014GL02531>.
- Chapman, S. C., N. W. Watkins, and D. A. Stainforth, 2019: Warming trends in summer heatwaves. *Geophys. Res. Lett.*, **46**, 1634–1640, <https://doi.org/10.1029/2018GL081004>.
- CRED, 2020: Natural disasters 2019: Now is the time to not give up. Centre for Research on the Epidemiology of Disasters, 8 pp., https://cred.be/sites/default/files/adrs_2019.pdf.
- Della-Marta, P. M., M. R. Haylock, J. Luterbacher, and H. Wanner, 2007: Doubled length of western European summer heat waves since 1880. *J. Geophys. Res.*, **112**, D15103, <https://doi.org/10.1029/2007JD008510>.
- Dole, R., and Coauthors, 2011: Was there a basis for anticipating the 2010 Russian heat wave? *Geophys. Res. Lett.*, **38**, L06702, <https://doi.org/10.1029/2010GL046582>.
- Dommenget, D., 2009: The ocean’s role in continental climate variability and change. *J. Climate*, **22**, 4939–4952, <https://doi.org/10.1175/2009JCLI2778.1>.
- Duchez, A., and Coauthors, 2016: Drivers of exceptionally cold North Atlantic Ocean temperatures and their link to the 2015 European heat wave. *Environ. Res. Lett.*, **11**, 074004, <https://doi.org/10.1088/1748-9326/11/7/074004>.
- DWD, 2021: Time series and trends. Accessed 22 September 2021, <https://www.dwd.de/EN/ourservices/zeitreihen/zeitreihen.html>.
- Eyring, V., S. Bony, G. A. Meehl, C. A. Senior, B. Stevens, R. J. Stouffer, and K. E. Taylor, 2016: Overview of the Coupled Model Intercomparison Project Phase 6 (CMIP6) experimental design and organization. *Geosci. Model Dev.*, **9**, 1937–1958, <https://doi.org/10.5194/gmd-9-1937-2016>.
- Fan, X., Q. Duan, C. Shen, Y. Wu, and C. Xing, 2020: Global surface air temperatures in CMIP6: Historical performance and future changes. *Environ. Res. Lett.*, **15**, 104056, <https://doi.org/10.1088/1748-9326/abb051>.
- Fischer, E. M., and C. Schär, 2010: Consistent geographical patterns of changes in high-impact European heatwaves. *Nat. Geosci.*, **3**, 398–403, <https://doi.org/10.1038/ngeo866>.
- Garrido-Perez, J. M., C. Ordóñez, R. García-Herrera, and J. L. Schnell, 2019: The differing impact of air stagnation on summer ozone across Europe. *Atmos. Environ.*, **219**, 117062, <https://doi.org/10.1016/j.atmosenv.2019.117062>.
- Hersbach, H., and Coauthors, 2020: The ERA5 global reanalysis. *Quart. J. Roy. Meteor. Soc.*, **146**, 1999–2049, <https://doi.org/10.1002/qj.3803>.
- Hoskins, B., and T. Woollings, 2015: Persistent extratropical regimes and climate extremes. *Curr. Climate Change Rep.*, **1**, 115–124, <https://doi.org/10.1007/s40641-015-0020-8>.
- IPCC, 2018: Global warming of 1.5°C. V. Masson-Delmotte et al., Eds., 630 pp., https://www.ipcc.ch/site/assets/uploads/sites/2/2019/06/SR15_Full_Report_High_Res.pdf.
- Jézéquel, A., P. Yiou, and S. Radanovics, 2018: Role of circulation in European heatwaves using flow analogues. *Climate Dyn.*, **50**, 1145–1159, <https://doi.org/10.1007/s00382-017-3667-0>.
- Junk, J., K. Goergen, and A. Krein, 2019: Future heat waves in different European capitals based on climate change indicators. *Int. J. Environ. Res. Public Health*, **16**, 3959, <https://doi.org/10.3390/ijerph16203959>.
- Kononov, I. B., M. Beekmann, I. N. Kuznetsova, A. Yurova, and A. M. Zvyagintsev, 2011: Atmospheric impacts of the 2010 Russian wildfires: Integrating modelling and measurements of an extreme air pollution episode in the Moscow region. *Atmos. Chem. Phys.*, **11**, 10031–10056, <https://doi.org/10.5194/acp-11-10031-2011>.
- Lesk, C., P. Rowhani, and N. Ramankutty, 2016: Influence of extreme weather disasters on global crop production. *Nature*, **529**, 84–87, <https://doi.org/10.1038/nature16467>.
- Ludwig, V., G. Spreen, C. Haas, L. Istomina, F. Kauker, and D. Murashkin, 2019: The 2018 North Greenland polynya observed by a newly introduced merged optical and passive microwave sea-ice concentration dataset. *Cryosphere*, **13**, 2051–2073, <https://doi.org/10.5194/tc-13-2051-2019>.
- Ma, F., X. Yuan, Y. Jiao, and P. Ji, 2020: Unprecedented Europe heat in June–July 2019: Risk in the historical and future context. *Geophys. Res. Lett.*, **47**, e2020GL087809, <https://doi.org/10.1029/2020GL087809>.
- Madruga de Brito, M., C. Kuhlicke, and A. Marx, 2020: Near-real-time drought impact assessment: A text mining approach on the 2018/19 drought in Germany. *Environ. Res. Lett.*, **15**, 1040a9, <https://doi.org/10.1088/1748-9326/aba4ca>.
- Miralles, D. G., P. Gentile, S. I. Seneviratne, and A. J. Teuling, 2019: Land–atmospheric feedbacks during droughts and heatwaves: State of the science and current challenges. *Ann. N. Y. Acad. Sci.*, **1436**, 19–35, <https://doi.org/10.1111/nyas.13912>.
- Mitchell, D., K. Kornhuber, C. Huntingford, and P. Uhe, 2019: The day the 2003 European heatwave record was broken.

- Lancet Planet. Health*, **3**, e290–e292, [https://doi.org/10.1016/S2542-5196\(19\)30106-8](https://doi.org/10.1016/S2542-5196(19)30106-8).
- Moore, G. W. K., A. Schweiger, J. Zhang, and M. Steele, 2018: What caused the remarkable February 2018 north Greenland polynya? *Geophys. Res. Lett.*, **45**, 13 342–13 350, <https://doi.org/10.1029/2018GL080902>.
- Perkins-Kirkpatrick, S. E., and S. C. Lewis, 2020: Increasing trends in regional heatwaves. *Nat. Commun.*, **11**, 3357, <https://doi.org/10.1038/s41467-020-16970-7>.
- Rodwell, M. J., and T. N. Palmer, 2007: Using numerical weather prediction to assess climate models. *Quart. J. Roy. Meteor. Soc.*, **133**, 129–146, <https://doi.org/10.1002/qj.23>.
- Russo, S., J. Sillmann, and E. M. Fischer, 2015: Top ten European heatwaves since 1950 and their occurrence in the coming decades. *Environ. Res. Lett.*, **10**, 124003, <https://doi.org/10.1088/1748-9326/10/12/124003>.
- Sánchez-Benítez, A., R. García-Herrera, D. Barriopedro, P. M. Sousa, and R. M. Trigo, 2018: June 2017: The earliest European summer mega-heatwave of reanalysis period. *Geophys. Res. Lett.*, **45**, 1955–1962, <https://doi.org/10.1002/2018GL077253>.
- , D. Barriopedro, and R. García-Herrera, 2020: Tracking Iberian heatwaves from a new perspective. *Wea. Climate Extremes*, **28**, 100238, <https://doi.org/10.1016/j.wace.2019.10.0238>.
- Schoetter, R., J. Cattiaux, and H. Douville, 2015: Changes of western European heat wave characteristics projected by the CMIP5 ensemble. *Climate Dyn.*, **45**, 1601–1616, <https://doi.org/10.1007/s00382-014-2434-8>.
- Schubert-Frisius, M., F. Feser, H. von Storch, and S. Rast, 2017: Optimal spectral nudging for global dynamic downscaling. *Mon. Wea. Rev.*, **145**, 909–927, <https://doi.org/10.1175/MWR-D-16-0036.1>.
- Sein, D. V., and Coauthors, 2017: Ocean modeling on a mesh with resolution following the local Rossby radius. *J. Adv. Model. Earth Syst.*, **9**, 2601–2614, <https://doi.org/10.1002/2017MS001099>.
- Semmler, T., and Coauthors, 2018: AWI AWI-CM1.1MR model output prepared for CMIP6 CMIP historical, Earth System Grid Federation, accessed 12 January 2021, <https://doi.org/10.22033/ESGF/CMIP6.2686>.
- , and Coauthors, 2019: AWI AWI-CM1.1MR model output prepared for CMIP6 ScenarioMIP ssp370, Earth System Grid Federation, accessed 12 January 2021, <https://doi.org/10.22033/ESGF/CMIP6.2803>.
- , and Coauthors, 2020: Simulations for CMIP6 with the AWI climate model AWI-CM-1-1. *J. Adv. Model. Earth Syst.*, **12**, e2019MS002009, <https://doi.org/10.1029/2019MS002009>.
- Seneviratne, S. I., and Coauthors, 2018: Land radiative management as contributor to regional-scale climate adaptation and mitigation. *Nat. Geosci.*, **11**, 88–96, <https://doi.org/10.1038/s41561-017-0057-5>.
- Shepherd, T. G., 2014: Atmospheric circulation as a source of uncertainty in climate change projections. *Nat. Geosci.*, **7**, 703–708, <https://doi.org/10.1038/ngeo2253>.
- , 2016: A common framework for approaches to extreme event attribution. *Curr. Climate Change Rep.*, **2**, 28–38, <https://doi.org/10.1007/s40641-016-0033-y>.
- , and Coauthors, 2018: Storylines: An alternative approach to representing uncertainty in physical aspects of climate change. *Climatic Change*, **151**, 555–571, <https://doi.org/10.1007/s10584-018-2317-9>.
- Sidorenko, D., and Coauthors, 2015: Towards multi-resolution global climate modeling with ECHAM6-FESOM. Part I: Model formulation and mean climate. *Climate Dyn.*, **44**, 757–780, <https://doi.org/10.1007/s00382-014-2290-6>.
- Sousa, P. M., R. M. Trigo, D. Barriopedro, P. M. M. Soares, and J. A. Santos, 2018: European temperature responses to blocking and ridge regional patterns. *Climate Dyn.*, **50**, 457–477, <https://doi.org/10.1007/s00382-017-3620-2>.
- , D. Barriopedro, R. García-Herrera, C. Ordóñez, P. M. M. Soares, and R. M. Trigo, 2020: Distinct influences of large-scale circulation and regional feedbacks in two exceptional 2019 European heatwaves. *Commun. Earth Environ.*, **1**, 48, <https://doi.org/10.1038/s43247-020-00048-9>.
- Stevens, B., and Coauthors, 2013: Atmospheric component of the MPI-M Earth system model: ECHAM6. *J. Adv. Model. Earth Syst.*, **5**, 146–172, <https://doi.org/10.1002/jame.20015>.
- Suarez-Gutiérrez, L., W. A. Müller, C. Li, and J. Marotzke, 2020: Dynamical and thermodynamical drivers of variability in European summer heat extremes. *Climate Dyn.*, **54**, 4351–4366, <https://doi.org/10.1007/s00382-020-05233-2>.
- Sutanto, S. J., C. Vitolo, C. Di Napoli, M. D'Andrea, and H. A. J. Van Lanen, 2020: Heatwaves, droughts, and fires: Exploring compound and cascading dry hazards at the pan-European scale. *Environ. Int.*, **134**, 105276, <https://doi.org/10.1016/j.envint.2019.105276>.
- Takhsa, M., O. Nikiéma, P. Lucas-Picher, R. Laprise, L. Hernández-Díaz, and K. Winger, 2018: Dynamical downscaling with the fifth-generation Canadian regional climate model (CRCM5) over the CORDEX Arctic domain: Effect of large-scale spectral nudging and of empirical correction of sea-surface temperature. *Climate Dyn.*, **51**, 161–186, <https://doi.org/10.1007/s00382-017-3912-6>.
- Trigo, R. M., R. García-Herrera, J. Díaz, I. F. Trigo, and M. A. Valente, 2005: How exceptional was the early August 2003 heatwave in France? *Geophys. Res. Lett.*, **32**, L10701, <https://doi.org/10.1029/2005GL022410>.
- van der Wiel, K., F. M. Seltén, R. Bintanja, R. Blackport, and J. A. Screen, 2020: Ensemble climate-impact modelling: Extreme impacts from moderate meteorological conditions. *Environ. Res. Lett.*, **15**, 034050, <https://doi.org/10.1088/1748-9326/ab7668>.
- van Garderen, L., F. Feser, and T. G. Shepherd, 2021: A methodology for attributing the role of climate change in extreme events: A global spectrally nudged storyline. *Nat. Hazards Earth Syst. Sci.*, **21**, 171–186, <https://doi.org/10.5194/nhess-21-171-2021>.
- van Niekerk, A., T. G. Shepherd, S. B. Vosper, and S. Webster, 2016: Sensitivity of resolved and parametrized surface drag to changes in resolution and parametrization. *Quart. J. Roy. Meteor. Soc.*, **142**, 2300–2313, <https://doi.org/10.1002/qj.2821>.
- Vautard, R., and Coauthors, 2020: Human contribution to the record-breaking June and July 2019 heatwaves in Western Europe. *Environ. Res. Lett.*, **15**, 094077, <https://doi.org/10.1088/1748-9326/aba3d4>.
- Vogel, M. M., R. Orth, F. Cheruy, S. Hagemann, R. Lorenz, B. J. J. M. van den Hurk, and S. I. Seneviratne, 2017: Regional amplification of projected changes in extreme temperatures strongly controlled by soil moisture–temperature feedbacks. *Geophys. Res. Lett.*, **44**, 1511–1519, <https://doi.org/10.1002/2016GL071235>.
- , J. Zscheischler, R. Wartenburger, D. Dee, and S. I. Seneviratne, 2019: Concurrent 2018 hot extremes across

- Northern Hemisphere due to human-induced climate change. *Earth's Future*, **7**, 692–703, <https://doi.org/10.1029/2019EF001189>.
- Voldoire, A., and Coauthors, 2019: Evaluation of CMIP6 DECK experiments with CNRM-CM6-1. *J. Adv. Model. Earth Syst.*, **11**, 2177–2213, <https://doi.org/10.1029/2019MS001683>.
- von Storch, H., H. Langenberg, and F. Feser, 2000: A spectral nudging technique for dynamical downscaling purposes. *Mon. Wea. Rev.*, **128**, 3664–3673, [https://doi.org/10.1175/1520-0493\(2000\)128<3664:ASNTFD>2.0.CO;2](https://doi.org/10.1175/1520-0493(2000)128<3664:ASNTFD>2.0.CO;2).
- Waldron, K. M., J. Paegle, and J. D. Horel, 1996: Sensitivity of a spectrally filtered and nudged limited-area model to outer model options. *Mon. Wea. Rev.*, **124**, 529–547, [https://doi.org/10.1175/1520-0493\(1996\)124<0529:SOASFA>2.0.CO;2](https://doi.org/10.1175/1520-0493(1996)124<0529:SOASFA>2.0.CO;2).
- Wang, Q., S. Danilov, D. Sidorenko, R. Timmermann, C. Wekerle, X. Wang, T. Jung, and J. Schröter, 2014: The Finite Element Sea Ice–Ocean Model (FESOM) v.1.4: Formulation of an ocean general circulation model. *Geosci. Model Dev.*, **7**, 663–693, <https://doi.org/10.5194/gmd-7-663-2014>.
- Wehrli, K., B. P. Guillod, M. Hauser, M. Leclair, and S. I. Seneviratne, 2018: Assessing the dynamic versus thermodynamic origin of climate model biases. *Geophys. Res. Lett.*, **45**, 8471–8479, <https://doi.org/10.1029/2018GL079220>.
- , —, —, —, and —, 2019: Identifying key driving processes of major recent heat waves. *J. Geophys. Res. Atmos.*, **124**, 11 746–11 765, <https://doi.org/10.1029/2019JD030635>.
- , M. Hauser, and S. I. Seneviratne, 2020: Storylines of the 2018 Northern Hemisphere heatwave at pre-industrial and higher global warming levels. *Earth Syst. Dyn.*, **11**, 855–873, <https://doi.org/10.5194/esd-11-855-2020>.
- Wiltshire, K. H., and Coauthors, 2010: Helgoland Roads, North Sea: 45 years of change. *Estuaries Coasts*, **33**, 295–310, <https://doi.org/10.1007/s12237-009-9228-y>.
- Woollings, T., and Coauthors, 2018: Blocking and its response to climate change. *Curr. Climate Change Rep.*, **4**, 287–300, <https://doi.org/10.1007/s40641-018-0108-z>.
- Zhang, K., and Coauthors, 2014: Technical note: On the use of nudging for aerosol–climate model intercomparison studies. *Atmos. Chem. Phys.*, **14**, 8631–8645, <https://doi.org/10.5194/acp-14-8631-2014>.
- Zhou, C., K. Wang, D. Qi, and J. Tan, 2019: Attribution of a record-breaking heatwave event in summer 2017 over the Yangtze River delta. *Bull. Amer. Meteor. Soc.*, **100**, S97–S103, <https://doi.org/10.1175/BAMS-D-18-0134.1>.